

See discussions, stats, and author profiles for this publication at: <https://www.researchgate.net/publication/282381078>

Effects of non-sinusoidal pitching motion on energy extraction performance of a semi-active flapping foil

Article in *Renewable Energy* · January 2016

DOI: 10.1016/j.renene.2015.07.037

CITATIONS
86

READS
466

4 authors:



Lubao Teng
Zhejiang University

5 PUBLICATIONS 235 CITATIONS

[SEE PROFILE](#)



Jian Deng
Zhejiang University

94 PUBLICATIONS 1,340 CITATIONS

[SEE PROFILE](#)



Dingyi Pan
Zhejiang University

53 PUBLICATIONS 1,079 CITATIONS

[SEE PROFILE](#)



Shao Xueming
Zhejiang University

127 PUBLICATIONS 2,427 CITATIONS

[SEE PROFILE](#)

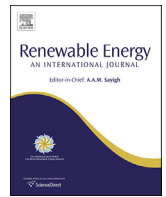
Some of the authors of this publication are also working on these related projects:



Project Biomimetic flying fish [View project](#)



Project Vortex rings and biomimetic propulsion (NSFC) [View project](#)



Effects of non-sinusoidal pitching motion on energy extraction performance of a semi-active flapping foil



Lubao Teng ^{a, b}, Jian Deng ^{a, b, *}, Dingyi Pan ^{a, b}, Xueming Shao ^{a, b}

^a State Key Laboratory of Fluid Power Transmission and Control, Zhejiang University, Hangzhou 310027, PR China

^b Department of Mechanics, Zhejiang University, Hangzhou 310027, PR China

ARTICLE INFO

Article history:

Received 9 March 2015

Received in revised form

13 July 2015

Accepted 13 July 2015

Available online xxx

Keywords:

Semi-active flapping foil

Non-sinusoidal profile

Energy extraction

ABSTRACT

Numerical simulations are used to study the energy harvester based on a semi-active flapping foil, in which the profile of the pitching motion is prescribed and the heaving motion is activated by the vertical hydrodynamic force. We consider a two-dimensional NACA0015 airfoil with the Reynolds number $Re = 1000$. First, for the sinusoidal pitching, an optimal combination of the parameters of pitching amplitude $\theta_0 = 75^\circ$ and reduced frequency $f^* = 0.16$ is identified, with the highest energy harvesting efficiency of 32% being recorded. Then we study non-sinusoidal pitching, with a gradual change from a sinusoid to a square wave as β is increased from one. We find that its effect of efficiency enhancement is limited for the parameters approaching their optimal values, and the upper boundary of the efficiency appears not to be increased. In detail, we report that when the pitching amplitude is small, non-sinusoidal pitching motions can indeed improve the performance of the system. However, when both the pitching amplitude and the flapping frequency are close to their optimal values, non-sinusoidal pitching motions contribute negatively to the harvesting efficiency. We suggest that a non-sinusoidal profile, at least a simple trapezoidal-like one is ineffective in the semi-active system reported by the current study.

© 2015 Elsevier Ltd. All rights reserved.

1. Introduction

Rivers and ocean are promising sources supplying people renewable and clean energy for their abundance of flow energy. Harvesting flow energy through flapping foil is a novel method inspired by aquatic animals, whose swimming is believed to have many advantages such as high speed, high efficiency and low noise [1]. Compared to traditional rotary turbines, the flapping foil system benefits from the simple idea of using translational motions instead of rotation, thus bringing about many advantages, e.g. it does not include fast rotating blades which are threats to aquatic animals, and it is easier to manufacture compared to the complicatedly shaped blades used in traditional turbines. Moreover, it is feasible to be planted in shallow water and in groups because their sweeping windows are rectangular [2].

It was originally declared that a flapping foil was capable of extracting energy from an unsteady current, such as a surface wave [3,4]. Decades ago, McKinney and DeLaurier [5] proposed the

concept of extracting flow energy through the flapping motion of an airfoil. Their original prototype was a windmill utilizing harmonically oscillating wing to extract wind energy. Usually, a flapping foil used for energy harvesting undergoes a coupled pitching and heaving motions. According to its degrees of freedom, this system can be categorized into three types, which are fully-active system, semi-active system and purely passive system respectively [6,7]. The performance of an energy harvester depends on its mechanical and kinematic parameters. The mechanical parameters include the pivoting location of the foil, the shape of the foil and the damping (for semi-active or fully passive systems). The kinematic parameters include the flapping frequency, the pitching amplitude, the heaving amplitude and the phase difference between the pitching and heaving motions. Extensive work has been carried out on fully-active systems [8–10]. Kinsey and Dumas [11] studied the power-extraction efficiency of a single oscillating airfoil with the reduced frequency in the range of 0–0.25 and pitching amplitude from 0° to 90°. In their studies, the efficiency reached as high as 35%. This high efficiency was also confirmed by experiments [12], in which two oscillating hydrofoils in tandem arrangement were tested. The rotating shaft driven by oscillating

* Corresponding author.

E-mail address: zjudengjian@zju.edu.cn (J. Deng).

hydrofoils was precisely controlled by an electrical drive, therefore a constant angular velocity was guaranteed. Moreover, it was reported that the energy harvesting efficiency of the flapping foil is related to the stability of the wake behind it [13]. The 'foil-wake resonance' coincides with the maximum energy harvesting efficiency. Performance of a flapping foil flow energy harvester in shear flows was investigated by Cho and Zhu [14]. It should be pointed out that the aspect ratios of foils are finite in realistic working conditions, though most previous research was based on 2-D assumptions. Shao et al. [15] investigated the wake structures of wings with different aspect ratios. Deng et al. [16] suggested that an aspect ratio around $AR = 4$ was the most appropriate choice for a real energy harvesting system with a sinusoidal pitching motion.

Though most of the above mentioned studies concentrated on fully-active flapping foil systems, semi-active system and fully passive system are more practical for energy harvesting. The performance of a semi-active flapping foil energy harvester has been investigated by Zhu and Peng [17]. They suggested that the performance depended on mechanical parameters including the magnitude of the damping and the location of the pitching axis, as well as operational parameters, e.g. the pitching frequency and pitching amplitude. A fully passive flapping foil system was examined by Peng and Zhu [18], who modeled the system by mounting a flapping foil on a damper and a rotational spring. Four different responses were recorded, and stable energy could be obtained when periodic pitching and heaving motions were both periodically excited. The response of a purely passive flapping foil flow energy harvester in a linear shear flow was also investigated [19]. It was indicated that in shear flows the devices were still capable of undergoing periodic responses as in uniform flows, which was essential for reliable energy harvesting. Young et al. [20] studied a fully passive flapping foil, declaring an efficiency as high as 41%. Huxham [21] conducted experiments on an oscillating foil energy converter undergoing a prescribed pitching motion with the heaving motion determined by unsteady hydrodynamic forcing on the foil.

In recent years, strategies to enhance energy extraction capacity have been reported. Wu et al. [22,23] found that the power extraction performance could be improved by placing the foil near a wall. Inspired by the observations that some animals such as turtles and birds flap their fins or wings in an asymmetrical fashion, people studied in-line motions of flapping foils which could cause high thrust and high efficiency [24,25]. Non-sinusoidal oscillating motions have also been introduced to enhance the efficiency of energy harvesting system. Xiao et al. [26] adopted a trapezoidal-like pitching profile, by varying the key parameter which controls the shape of the pitching profile they found an optimal profile which was proved to dramatically increase the power output and energy harvesting efficiency over a wide range of Strouhal numbers. Ashraf et al. [27] reported that 15% enhancement of efficiency could be achieved by adopting non-sinusoidal pitch-plunge motions. A comparison between the effects of different non-sinusoidal motions was carried out by Lu et al. [28]. They found that an appropriate combination of non-sinusoidal pitching and non-sinusoidal plunging motions had the potential to provide the best energy harvesting performance. According to the numerical simulations by Xie et al. [29], they believed that relatively high flapping frequency and large pitching amplitude should be chosen for the best energy harvesting performance. Though all studies reviewed above focused on fully-active flapping foils, their efforts indicate a possibility of increasing the efficiency of a semi-active harvester by adopting non-sinusoidal pitching motions. However, we note that none of these studies has covered the optimal parametric range in which the highest efficiency for sinusoidal motion has already been achieved. We list their chosen parameters as the

following. In the study by Xiao et al. [26], two nominal angles of attack, $\alpha_0 = 10^\circ$ and $\alpha_0 = 20^\circ$, were adopted. Lu et al. [28] selected a nominal angle of attack $\alpha_0 = 15^\circ$. Xie et al. [29] covered the range of pitching amplitude θ_0 from 0° to 35° . According to the report by Kinsey [11], these parameters are out of the best-performance parametric range. As pointed out by Deng et al. [16] that the increasing effect of non-sinusoidal pitching amplitude on efficiency was weak as θ_0 approaching its optimal value. Platzer et al. [30] also indicated that the feasibility of efficiency enhancement by non-sinusoidal motions at different operation parameters had not been well investigated. Therefore, clarification on this issue is needed by adopting a wider parameter range.

In this paper, we use numerical code based on finite-volume method to solve the two-dimensional Navier–Stokes equations. The flow by a semi-active flapping foil is simulated with prescribed pitching profiles while the heaving motion is determined by the hydrodynamic force acting on the foil. We consider a two-dimensional NACA0015 foil, with the Reynolds number of 1000 calculated by the incoming flow velocity, the chord length and the properties of the fluid. As a basis for further investigations, firstly, we carry out a parametric study on a flapping foil with sinusoidal pitching motion. In order to study the appropriateness of non-sinusoidal pitching motions on improving the energy extraction performance of a semi-active system, we consider both small pitching amplitudes and high pitching amplitudes, which we believe cover an adequately large range from low harvesting efficiencies to high harvesting efficiencies. Two representative pitching amplitudes $\theta_0 = 45^\circ$ and $\theta_0 = 75^\circ$ are investigated in detail.

2. Problem description and numerical methods

2.1. Kinematic motion of the foil

We consider a two-dimensional NACA0015 airfoil, as shown in Fig. 1. The chord length of the foil is a . The pivoting point is located at the center line of the foil with a distance b from the leading edge, which is one third of the chord length in this paper. The upstream flow velocity is denoted by U . The pitching angle is denoted by θ . The translational displacement of the pivoting point from the origin in y -direction is h . The energy converting device is represented as a constant damping c . The foil performs combined motions of pitching and heaving, and the pitching profile is expressed as:

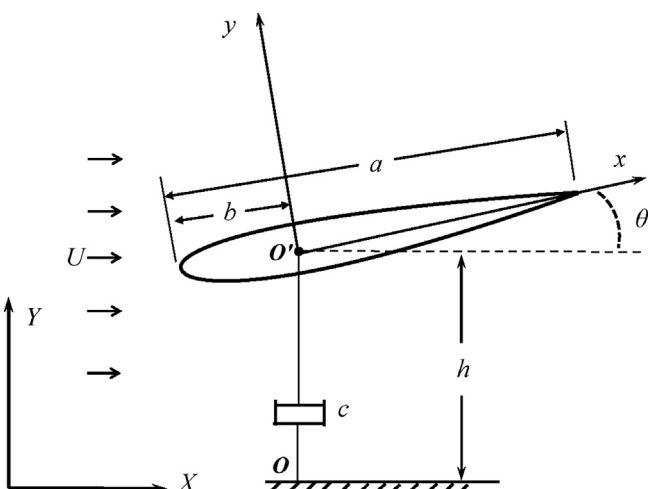


Fig. 1. Schematic of the energy harvester by a semi-active flapping foil.

$$\theta = \begin{cases} \theta_0 \sin(\beta \omega t), & 0 \leq t \leq \frac{\pi}{2\beta\omega}; \\ \theta_0, & \frac{\pi}{2\beta\omega} < t \leq \frac{\pi}{2\omega} \left(2 - \frac{1}{\beta}\right); \\ \theta_0 \sin[\beta \omega t + \pi(1 - \beta)], & \frac{\pi}{2\omega} \left(2 - \frac{1}{\beta}\right) < t \leq \frac{\pi}{2\omega} \left(2 + \frac{1}{\beta}\right); \\ -\theta_0, & \frac{\pi}{2\omega} \left(2 + \frac{1}{\beta}\right) < t \leq \frac{\pi}{2\omega} \left(4 - \frac{1}{\beta}\right); \\ \theta_0 \sin[\beta \omega t + 2\pi(1 - \beta)], & \frac{\pi}{2\omega} \left(4 - \frac{1}{\beta}\right) < t \leq \frac{2\pi}{\omega}, \end{cases} \quad (1)$$

where the angular flapping frequency $\omega = 2\pi f$, and we also define a reduced frequency $f^* = fa/U$. It is noted that when $\beta = 1$, the foil pitches sinusoidally, while the pitching profile tends to be trapezoidal as $\beta \rightarrow \infty$. In Fig. 2, we plot the time variation of the pitching profile $\theta(t)$ for some typical values of β . There is a gradual change from a sinusoid to a square wave as β increases from one. The heaving motion is determined by

$$m\ddot{h} + c\dot{h} = F_y, \quad (2)$$

where m represents the mass of the foil, c represents the constant damping and F_y represents the total force acting on the foil in y -direction. In this paper, the mass of the foil is fixed, so that the density ratio between the foil and fluid is fixed as well, which is $\rho_{\text{foil}}/\rho_{\text{fluid}} = 4.72$. This density ratio is practically reasonable, if we assume that the foil is made of a kind of material with the density between steel and aluminum. We set the damping to be 3.14, according to [17], in which the optimal damping of $c^* = \pi$ was identified by a potential-flow based thin plate model.

The combination of the two motions results in, with respect to the incoming flow, an effective Angle of Attack (AoA) [11], which can be formulated as

$$\alpha(t) = \arctan(V_y(t)/U_\infty) - \theta(t), \quad (3)$$

where $V_y(t)$ is the heaving velocity, or vertical velocity in y -direction of the foil.

2.2. Parametrization of energy harvesting

The instantaneous power input actuating the pitching motion of the foil can be calculated by $P_i(t) = -M(t)\Omega(t)$, where M is the torque

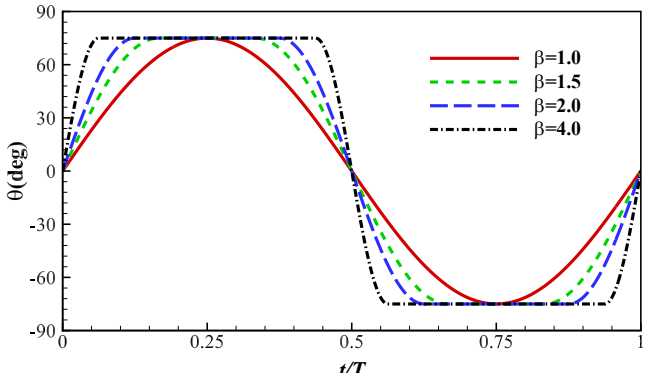


Fig. 2. Variation of instantaneous pitching angle $\theta(t)$ over one period for different β as defined in Eq. (1) ($\theta_0 = 75^\circ$).

about the pivoting point, and Ω is the angular velocity of the foil. The power output is achieved by the damping c , and can be calculated as $P_o(t) = ch^2$. The net power (or total power) is thus given by $P = P_o - P_i$. Dimensionless coefficients for force, torque and power, including power output, power input and net power (or total power) are defined as

$$C_Y = \frac{Y}{1/2\rho U_\infty^2 ba}, \quad C_M = \frac{M}{1/2\rho U_\infty^2 ba^2}, \quad (4)$$

$$C_{P_o} = \frac{P_o}{1/2\rho U_\infty^3 ba}, \quad C_{P_i} = \frac{P_i}{1/2\rho U_\infty^3 ba}, \quad C_P = \frac{P}{1/2\rho U_\infty^3 ba}, \quad (5)$$

where a is the chord of the foil, b is the foil span (here, for two-dimensional situation we consider an arbitrary length b of the airfoil), d is the overall vertical extent of the foil motion calculated as the distance in y -direction between the highest position and the lowest position reached by the foil, either the leading edge or the trailing edge, Y is the vertical hydrodynamic force or lift, and M is the torque. The time-averaged power is denoted by $\langle P \rangle$, and its coefficient by $\langle C_P \rangle$. The total energy harvesting efficiency η is defined as the portion of the flow energy within the working plane that extracted by the harvester:

$$\eta = \frac{\langle P \rangle}{\frac{1}{2}\rho U_\infty^3 bd}, \quad (6)$$

2.3. Numerical methods and validation

The flow field is simulated by an open source code OpenFOAM [31]. The time-dependent Navier–Stokes equations are solved using finite-volume method. In order to speed computation time we choose the Reynolds number to be 1000 thus no turbulence model needs to be used. Moreover, the flow is assumed incompressible. The governing equations are solved on a moving grid domain using the Arbitrary Lagrangian Eulerian (ALE) formulation [32]. The integral form of the governing equations defined in an arbitrary moving volume V bounded by a closed surface S is

$$\frac{d}{dt} \int_V \rho \mathbf{U} dV + \oint_S \mathbf{ds} \cdot \rho (\mathbf{U} - \mathbf{U}_b) \mathbf{U} = \oint_S \mathbf{ds} \cdot (-p \mathbf{I} + \rho \nu \nabla \mathbf{U}), \quad (7)$$

where, ρ is the density, \mathbf{U} is the fluid velocity, p is the pressure, and ν is the kinematic viscosity. As the volume V is no longer fixed in space, its motion is captured by the motion of its bounding surface S with the boundary velocity \mathbf{U}_b . For details of the discretization and implementation of boundary conditions, as well as the transformation of the underlying partial differential equations into the corresponding systems of algebraic equations, one can refer to Feriger and Peric [32].

The space discretizations are second-order upwind for the convection terms and central differences for the Laplacian terms, respectively. The time discretization is the first-order implicit Euler scheme. The pressure–velocity coupling is achieved by PISO algorithm [32]. For the resulting algebraic equations after discretization, the preconditioned conjugate gradient (PCG) method is used to treat the pressure equation and the preconditioned bi-conjugate gradient (PBiCG) method for the momentum equations. Numerical accuracy is set to double-precision and the initial conditions are chosen to be uniform. We set the boundary condition on the foil to be moving-wall, with zero flux normal to the wall. The velocity U_∞ at the far field is kept constant.

The explicit Runge–Kutta method is used to compute the transverse displacement, and the moving velocity of the foil, as shown below:

$$h^{n+1} = h^n + \frac{1}{6}(K_1 + K_2 + K_3 + K_4)\Delta t, \quad (8)$$

$$\dot{h}^{n+1} = \dot{h}^n + \frac{1}{6}(L_1 + L_2 + L_3 + L_4)\Delta t, \quad (9)$$

where

$$\begin{cases} K_1 = \dot{h}^n, L_1 = \frac{-b}{m} + \frac{F_y}{m}, \\ K_2 = \dot{h}^n + \frac{\Delta t}{2}L_1, L_2 = \frac{-b}{m}\left(\dot{h}^n + \frac{\Delta t}{2}L_1\right) + \frac{F_y}{m}, \\ K_3 = \dot{h}^n + \frac{\Delta t}{2}L_2, L_3 = \frac{-b}{m}\left(\dot{h}^n + \frac{\Delta t}{2}L_2\right) + \frac{F_y}{m}, \\ K_4 = \dot{h}^n + \frac{\Delta t}{2}L_3, L_4 = \frac{-b}{m}\left(\dot{h}^n + \frac{\Delta t}{2}L_3\right) + \frac{F_y}{m}. \end{cases} \quad (10)$$

To validate the Navier–Stokes solver, we carry out self-consistency tests to assure the satisfactory independence of the force calculations with respect to both spacial and temporal discretization. To validate the time-discretization independence, we simulate on three different time steps, 5×10^{-5} (9.09×10^4 steps per cycle), 1×10^{-4} (4.5×10^4 steps per cycle) and 2×10^{-4} (2.27×10^4 steps per cycle) respectively. The results at $f^* = 0.2$ and $\theta_0 = 75^\circ$ are presented in Table 1. It shows that the results by three different time steps are close to each other and the largest difference of η between different cases is less than 0.5%. We plot the variations over time of lift force coefficients and pitching moment coefficients, as shown in Fig. 3(a) and (b) respectively, showing little variation among different time steps. Hence, the moderate time step of 1×10^{-4} is small enough to guarantee temporal accuracy. Then, we simulate on three different meshes: coarse mesh (89846 cells), medium mesh (151292 cells) and fine mesh (305256 cells). The energy harvesting efficiency calculated by the coarse, medium and fine mesh are 27.62%, 27.65% and 27.69% respectively. The difference between the medium mesh and the fine mesh is less than 0.2%. Therefore, we adopt the medium mesh of 151292 cells in the following simulations. For more details about numerical validation one can refer to our previous study on a flapping foil with prescribed motions [16].

3. Results and discussions

In this section, the results with a sinusoidal pitching profile will be presented firstly. The effects of pitching amplitude and pitching frequency will both be examined. The optimal parametric combinations for high efficiencies will be identified. Then, we focus on the effects of non-sinusoidal pitching profiles, with small and large pitching amplitudes being considered respectively.

Table 1
The simulation results for different time steps ($f^* = 0.2, \theta_0 = 75^\circ$).

Time step	P_i	P_o	η
5×10^{-5}	0.131984	0.460921	0.276167
1×10^{-4}	0.131949	0.461382	0.276512
2×10^{-4}	0.132097	0.462494	0.277168

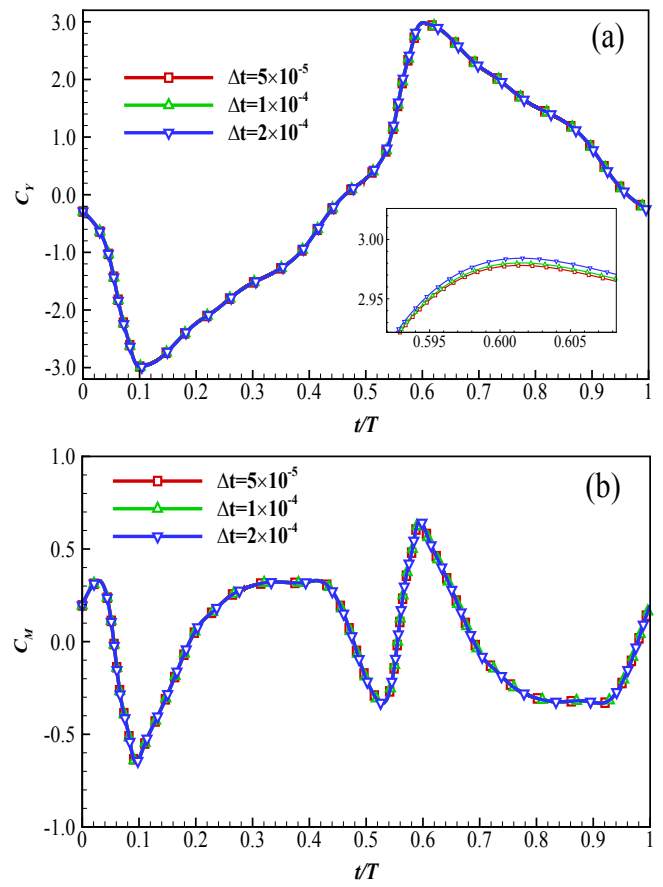


Fig. 3. Variation over time for a periodic cycle for two-dimensional flow cases for validation at different time resolutions (denoted by different symbols) of: (a) lift force coefficients, with a zoom-in view near the peak lift, and (b) pitching moment coefficients (at the x axis location marked on Fig. 1) as defined in Eq. (4).

3.1. Results of sinusoidal pitching profile

To identify the highest efficiency for sinusoidal pitching, we carry out a parametric study on the (f^*, θ_0) space. After extensive simulations we conjecture that the highest efficiency lies in the parametric range of $\theta_0 = 70^\circ – 80^\circ$ and $f^* = 0.12 – 0.16$. We show the energy harvesting efficiency versus flapping frequency for $\theta_0 = 70^\circ$, $\theta_0 = 75^\circ$ and $\theta_0 = 80^\circ$ in Fig. 4. It shows that the maximum energy harvesting efficiencies are achieved at the flapping frequency $f^* = 0.16$ for all three pitching amplitudes. The variation of

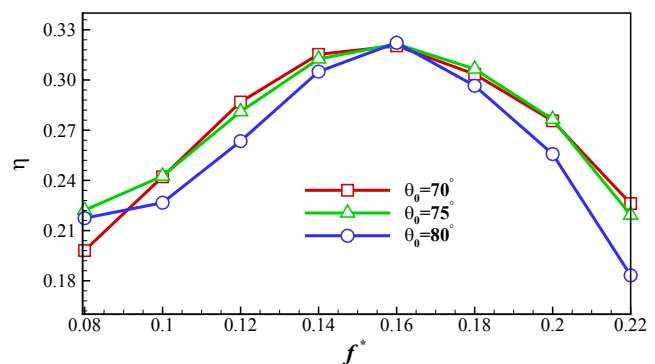


Fig. 4. Variations of energy harvesting efficiency with flapping frequency for different pitching amplitudes.

energy harvesting efficiency versus the pitching amplitude at $f^* = 0.16$ is shown in Fig. 5. The highest efficiency is identified in the range of $\theta_0 = 70^\circ–80^\circ$. The result for $\theta_0 < 60^\circ$ in Fig. 5 is consistent with that obtained by thin-plate model [17], which predicted a monotonic increase of the efficiency as $\theta_0 < 60^\circ$ and a highest efficiency of 27% achieved at $\theta_0 = 60^\circ$. We note that $\theta_0 = 60^\circ$ is also the upper boundary of Zhu & Peng's calculations [17]. It is interesting to observe in Fig. 5 that the efficiency varies little in the range of $\theta_0 = 70^\circ–80^\circ$ where the highest efficiency of 32% is achieved.

It should be pointed out that we assume that the density ratio between the foil and its surrounding fluid is 4.72, which might lead to an efficiency degradation compared to a massless foil [33].

3.2. Effects of non-sinusoidal pitching motions

According to Section 1 we have known that the motivation of the current study comes from two aspects. First, all previous studies on the effects of non-sinusoidal motions on energy harvesting were about fully-active system. Second, most of them concentrated on low efficiency situations, of which the non-sinusoidal motions have been proved to be effective. As reported by Xiao et al. [26], who selected two small nominal angles of attack (10° and 20°), non-sinusoidal profiles of pitching motion lead to significant increments of both net power output and energy harvesting efficiency. However, it is still not clear if this strategy applies to high efficiency situations. In another word, it is not clear if the peak efficiency can be increased by engaging non-sinusoidal motions. By studying the effects of finite spans, Deng et al. [16] pointed out that the efficiency enhancement by varying β might be limited for the cases that θ_0 approaches its optimal value i.e. $\theta_0 = 81.5^\circ$.

In Section 3.1 we have identified optimal parameters for high efficiencies with sinusoidal pitching motion, which are within the range of $\theta_0 \in [70^\circ, 80^\circ]$ and $f^* \in [0.12, 0.16]$, in which the best performance of the system can be achieved. To get a comprehensive understanding of the effects of non-sinusoidal motion, here we study both low efficiency situations by choosing small pitching amplitudes and high efficiency situations by choosing large pitching amplitudes. Their different responses to non-sinusoidal pitching will be discussed in detail.

3.2.1. Small pitching amplitudes

The energy harvesting efficiency versus β for various pitching frequencies at $\theta = 45^\circ$ is shown in Fig. 6, in which the dotted line marks the highest energy harvesting efficiency obtained by sinusoidal pitching motion as discussed in Section 3.1, which is about 0.32. We observe that there exist maximum values of the energy harvesting efficiencies for each frequency. The same trend is found

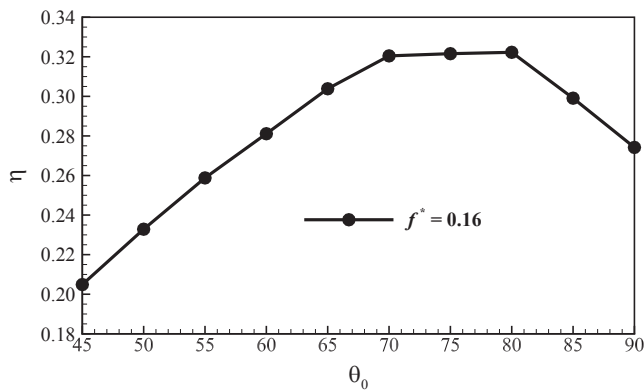


Fig. 5. Variation of energy harvesting efficiency with pitching amplitude at $f^* = 0.16$.

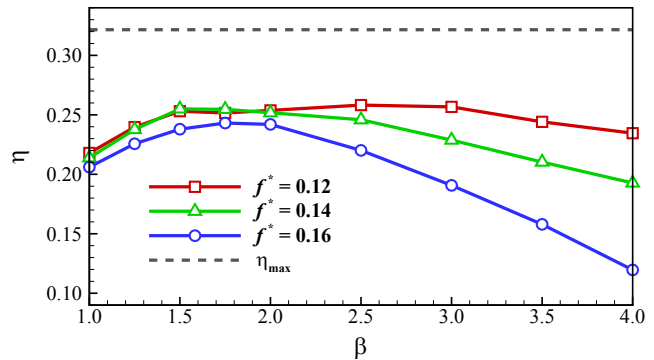


Fig. 6. Energy harvesting efficiency η versus β for different pitching frequencies at $\theta_0 = 45^\circ$, with the dashed line implying the highest efficiency achieved by sinusoidal pitching.

in Fig. 7, which presents the variation of time-averaged net power output with β for the three pitching frequencies. We note that the efficiency η is defined as the net power output over the incoming kinematic energy of the swept area of the flapping foil, therefore it is possible that η and $\langle P \rangle$ reach their maximum values at different β as shown in Figs. 6 and 7 respectively. It implies at least from Fig. 7 that the increment of power output is reduced as approaching the optimal frequency ($f^* = 0.16$ in the current study).

To take a close-up examination on the effects of non-sinusoidal pitching profiles, we present the two components contributing to the net power output for $f^* = 0.16$ in Fig. 8. We observe that the power output increases with β , while the power input varies little for $\beta < 2.0$ and increases with β for $\beta > 2.0$. It indicates that for large β , the power required to yaw the foil increases though its power output increases as well. Competition between positive contributions and negative contributions to the net power output reaches a compromised maximum efficiency over various β , as shown in Fig. 6. For $f^* = 0.16$, the maximum efficiency is 0.24, which is a 16.5% higher from its value at $\beta = 1.0$ or its sinusoidal counterpart.

We present time histories of the lift force coefficients and the heaving velocities during a cycle for $\beta = 1.0$, $\beta = 1.5$ and $\beta = 2$ in Fig. 9. The plots show the fifth cycle in the simulations, by which time the flow appears to have reached a stationarily periodic oscillating state for both the hydrodynamic forces and the flow fields. For $\beta = 1.0$, the magnitude of the lift force has a peak twice in each cycle. We observe that as β increases, i.e. approaching a trapezoidal wave, the time history of lift force changes its shape from sinusoidal-like to trapezoidal-like, with two peaks appearing instead of a single peak. The peak value has also been increased,

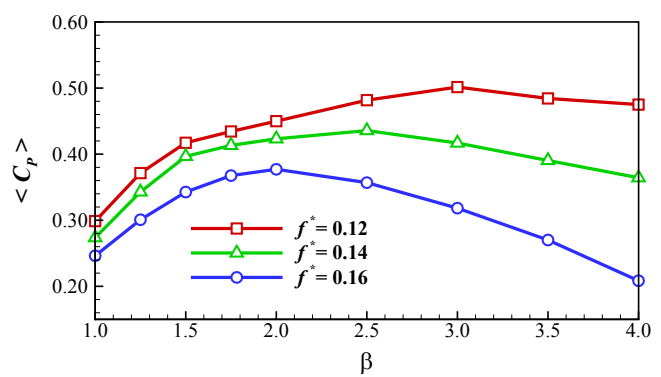


Fig. 7. Time-averaged net power $\langle C_p \rangle$ versus β for different pitching frequencies at $\theta_0 = 45^\circ$.

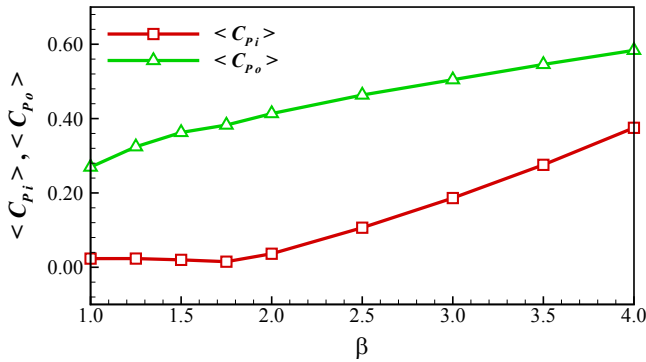


Fig. 8. Time-averaged power input $\langle C_{p_i} \rangle$ and power output $\langle C_{p_o} \rangle$ versus β ($\theta_0 = 45^\circ$, $f^* = 0.16$).

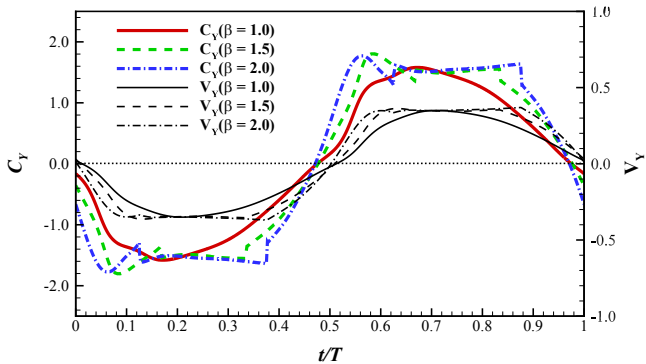


Fig. 9. Variations of lift force coefficient and heaving velocity over one period for different pitching profiles ($\theta_0 = 45^\circ$, $f^* = 0.16$), with the dotted line denoting the zero value.

which appears earlier than the single peak. This qualitative behavior of peaking secondarily in each cycle has also been reported for purely active system [11]. We note that the effective Angle of Attack (AoA) changes as β varies, and reaches 26° during the cycle for all β , while for the larger β there is relatively longer time interval with the effective AoA close to its maximum magnitude, as shown in Fig. 10. With such a large value of AoA, it is no surprise to observe dynamic-stall vortex shedding taking place during the motion. Although boundary-layer separation leads to unfavorable effects in stationary aerodynamics, dynamic-stall vortex shedding typically contributes to improved performance, and as

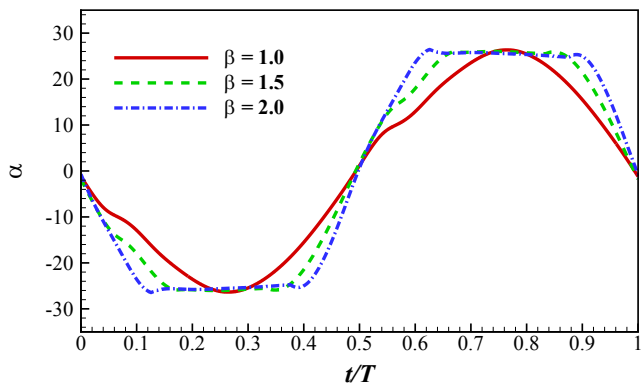


Fig. 10. Variation of effective angle of attack over one period for different pitching profile ($\theta_0 = 45^\circ$, $f^* = 0.16$).

reported [16] that LEVs are expected to occur during the cycles of most of the efficient cases. We further note that there exists a phase difference between the lift force and the vertical velocity, indicated by that the lift curves cross the zero value line away from the point that the heaving velocity changes its sign. This might be due to the inertial effects, as implied by Eq. (2). Nevertheless they both predict the same response to the variation of β that the lift forces and vertical velocities are larger for $\beta = 1.5$ and $\beta = 2.0$ than that of $\beta = 1.0$ for almost all time. Though there is no measurable growth for the peak value of vertical velocity for $\beta = 1.5$ and $\beta = 2.0$ compared to $\beta = 1.0$, the harvester benefits from its persistence over a long time interval, leading to significant growth of the power output as shown in Fig. 8.

It is important to appreciate that the magnitude of the power input is substantially smaller than the power output for $1.0 < \beta < 2.0$, as shown in Fig. 8, therefore the evaluation of the efficiency enhancement has been simplified to examine the power output, at least in this parametric range.

Unsurprisingly, from the dependence of the energy harvesting performance on the effective AoA as revealed by previous studies [26,28,29], non-sinusoidal can indeed increase the energy harvesting efficiency by modifying the profile of AoA. However, we should point out that $\theta_0 = 45^\circ$ is not optimal for energy harvesting. For small pitching amplitudes, the energy harvesting efficiency through tuning β is far below that obtained by optimization of the parameters of sinusoidal pitching motion which is marked by the dashed line in Fig. 6. This phenomenon reminds us to investigate the effects of increasing β when the pitching amplitude is close to its optimal value of obtaining the highest energy harvesting efficiency for sinusoidal pitching.

3.2.2. Large pitching amplitudes

It is not established that non-sinusoidal pitching motions can increase the upper boundary of energy harvesting efficiency, though they indeed increase the efficiency of non-optimal cases as discussed above, it is not at all clear whether this effect carries over to optimal cases. In this section, we choose $\theta_0 = 75^\circ$, at which the highest efficiency is achieved for sinusoidal pitching as shown in Figs. 4 and 5.

We present the energy harvesting efficiency versus β for different pitching frequencies at $\theta_0 = 75^\circ$ in Fig. 11. It shows that the efficiency is increased by 23% for $f^* = 0.12$ as increasing β , to a value slightly below the highest efficiency of sinusoidal pitching marked by the dashed line, while for $f^* = 0.14$ and $f^* = 0.16$ the improvement of the energy extraction efficiency obtained by tuning β is not effective at all. It thereby indicates that the efficiency enhancement by replacing sinusoidal pitching waveforms with non-sinusoidal waveforms does not apply to optimal parameters.

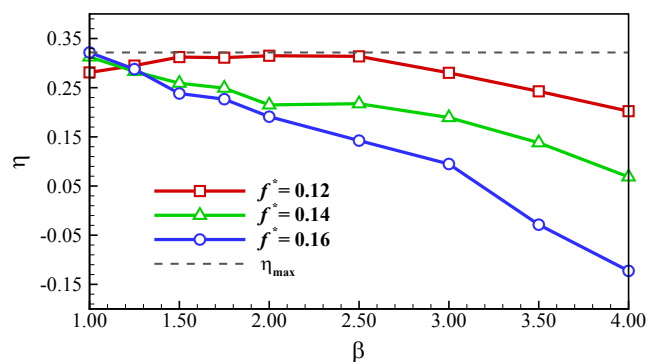


Fig. 11. Energy harvesting efficiency η versus β for different pitching frequencies with $\theta_0 = 75^\circ$ and $f^* = 0.16$.

We present the time-averaged power input and power output varying with β for $\theta_0 = 75^\circ$ and $f^* = 0.16$ in Fig. 12. Apparently different from the cases for small pitching amplitudes as shown in Fig. 8, in Fig. 12 the power output varies little for $1.0 < \beta < 2.0$ while the power input increases monotonically with increasing β , and the power input grows faster than the power output with β , resulting in a monotonic decreasing of the net power with β and the reduction of efficiency as shown in Fig. 11. It indicates that the positive contributions from the heaving motion can actually be overwhelmed by rapidly increased power required for the pitching motion. An extreme example of this is the case shown in Fig. 12 at $\beta = 4.0$, at which point the power required to yaw the foil is even larger than that gained by heaving motion.

To further understand the reduction of efficiency enhancement, we present the lift force coefficient over one period for $\theta_0 = 75^\circ$ and $f^* = 0.16$ in Fig. 13. We find a significant increase in the lift force at the peak as β increases from $\beta = 1.0$ to $\beta = 2.0$. Indeed, for $\beta = 2.0$ the peak value for lift is 54% larger than that found for a flow with $\beta = 1.0$, and this peak appears a little earlier in the cycle. This shift in the timing of the peak in lift force appears to be related to changes in the angle of attack as β varies, as shown in Fig. 14. It is noted that the peak value of lift force occurs when the effective AoA is 17° for $\beta = 2.0$, and 19.8° for $\beta = 1.5$, while the peak is associated with a larger AoA of 30.7° when $\beta = 1.0$. Immediately after $t/T = 0.5$, the effective angle of attack for $\beta = 2.0$ increases more rapidly than $\beta = 1.0$. As has been extensively discussed by previous studies [25] about the relationship between effective angle of attack and the highest lift force achieved by flapping foil, there appears to be two competitive effects. The rapid increase of angle of attack at a high angle of attack induces stall delay, which helps the flow remain substantially attached to the foil to a significantly higher angle of attack than can be achieved in steady-state conditions. Conversely, a higher pitching rate increases the highest value of lift, and brings about earlier stall than a lower pitching rate. We observe in Fig. 13 that immediately after the peaks, the lift forces drop dramatically to relatively lower values for $\beta = 1.5$ and $\beta = 2.0$ compared to $\beta = 1.0$. The same trend is found in the time histories of vertical velocities, which are directly related to power outputs. By comparing Fig. 13 with the cases with small pitching amplitudes as shown in Fig. 9, we find a marked qualitative difference. For $\beta = 1.5$ and $\beta = 2.0$ with small pitching amplitudes, after the 'primary' peak the lift drops slightly and then rises up again, and increases gradually to a 'secondary' peak, as shown in the range of $t/T = 0.8 – 0.9$ in Fig. 9.

3.2.3. Wake topology of non-sinusoidal pitching cases

We wish to develop an understanding of the physical mechanism of the effect of variation of β , in Fig. 15 we plot the vorticity

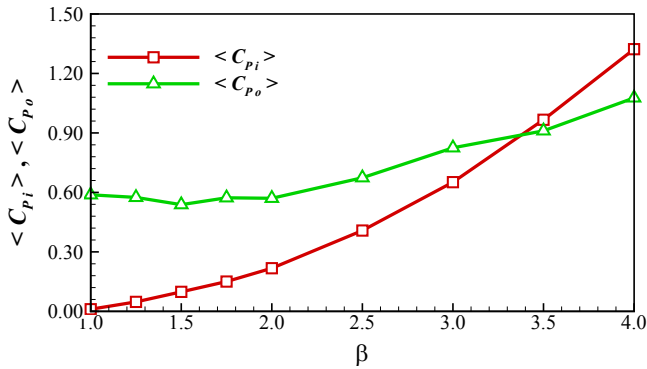


Fig. 12. Time-averaged power input $\langle P_i \rangle$ and power output $\langle P_o \rangle$ versus β ($\theta_0 = 75^\circ$, $f^* = 0.16$).

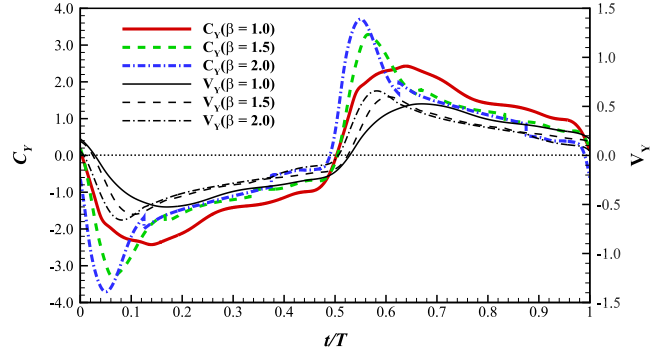


Fig. 13. Variations of lift force coefficient over one period for different pitching profile ($\theta_0 = 75^\circ$, $f^* = 0.16$).

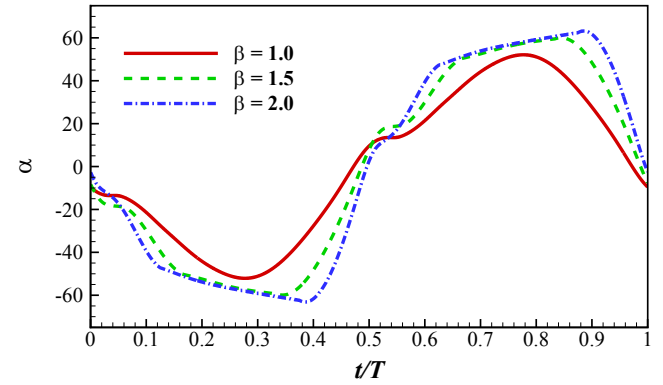


Fig. 14. Variations of effective angle of attack over one period for different pitching profiles ($\theta_0 = 75^\circ$, $f^* = 0.16$).

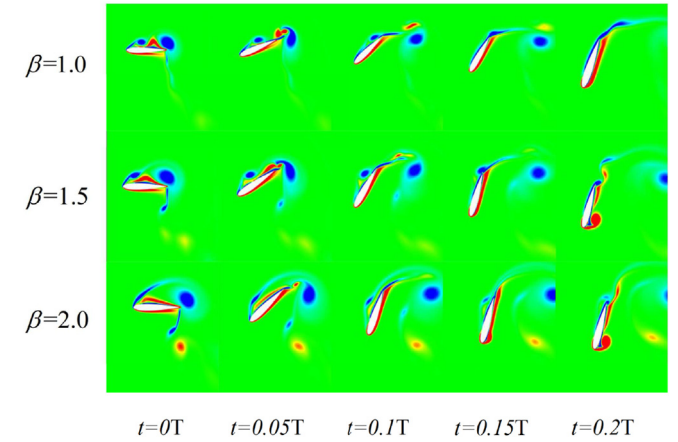


Fig. 15. Vortex topology of five instants between $t = 0T$ and $t = 0.2T$ for flows with $\beta = 1$, $\beta = 1.5$, and $\beta = 2.0$, represented by contour levels of spanwise vorticity ranging from -15 (darker grey) to 15 (lighter grey). The pitching amplitude is $\theta_0 = 75^\circ$ and the flapping frequency is $f^* = 0.16$.

contours between $t = 0T$ and $t = 0.2T$ during which the lift force dramatically changes as shown in Fig. 13. Five instants are included in this plot. The corresponding pressure contours are shown in Fig. 16. First, at $t = 0$, the Leading Edge Vortex (LEV) has traveled to the trailing edge of the foil for $\beta = 1.0$ but is still attached to the foil, while for $\beta = 2.0$ it has separated from the foil, indicating different timings of vortex shedding with varying β . We also notice that there is a small leading vortex formed at $t = 0$ and then travels

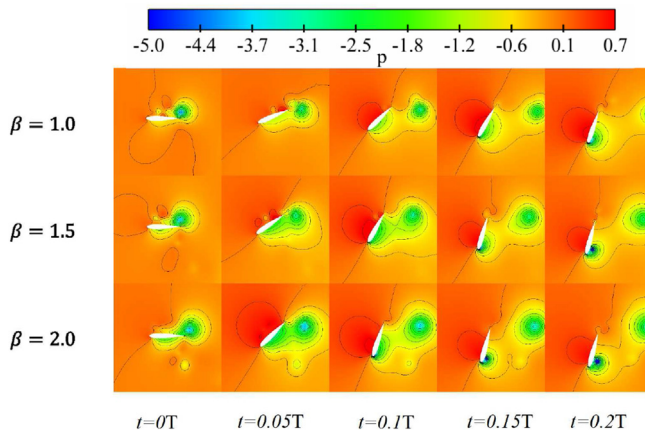


Fig. 16. Pressure contours of five instants between $t = 0T$ and $t = 0.2T$ for flows with $\beta = 1$, $\beta = 1.5$, and $\beta = 2.0$. The pitching amplitude is $\theta_0 = 75^\circ$ and the flapping frequency is $f^* = 0.16$.

downstream along the upper surface of the foil in the time interval of $t = 0 - 0.1T$, which is stronger for $\beta = 1.0$ than $\beta = 2.0$, as apparently shown at $t = 0.05T$ and $t = 0.1T$ in Fig. 15. This good attachment of the flow during this time interval is due to the so-called stall delay. We also note that the lift forces behave differently against effective angle of attacks for different β . This may be caused by the Kramer effect and it is also related to the leading edge vortex. We further note that during $t = 0.1T - 0.2T$ for $\beta = 1$ the flow is attached well to both the upper and lower surfaces of the foil, indicating the retaining of the lift force at a high level in this time interval, while for $\beta = 1.5$ and $\beta = 2.0$ a leading vortex is forming below the foil, the corresponding forces thereby drop rapidly because actual stall happens as shown in Fig. 13. We note that the leading edge vortex attached to the surface of the foil when traveling along the surface can somewhat keep the lift force at a high level, but it cannot compare with the primary lift peak as shown at $t = 0.05T$ for $\beta = 2.0$ in Fig. 13. According to the discussion above, particularly the comparison between small pitching amplitude (see Fig. 9) and large pitching amplitude (see Fig. 13), we find that for larger pitching amplitude, the benefit gained from the leading edge vortex has been degraded when increasing β . This is intuitive if we compare the time interval $t = 0.1T - 0.2T$ for $\beta = 2.0$ in Fig. 13 to that in Fig. 9.

The different vortical evolutions for various β remind us that the flow around a flapping foil is complicated and strongly related to unsteady hydrodynamics. The good performance of this energy harvesting system by applying sinusoidal pitching is achieved by tuning the flow to an appropriate forming of the leading vortex and a good timing of its shedding from the foil. For low efficiency cases, as represented in this paper by small pitching amplitudes, the flow can be indeed tuned to a better one by implementing non-sinusoidal pitching motions. However, for the already optimal flow, the performance improvement by non-sinusoidal pitching motions is very limited.

4. Conclusions

In this paper, we have studied the effects of non-sinusoidal pitching motions on an energy harvester by semi-active flapping foil. The incompressible Navier–Stokes equations are solved using a finite-volume based numerical solver with a moving grid technique. Both sinusoidal and trapezoidal pitching profiles are investigated. First, we identify an optimal range of parameters of $\theta_0 = 70^\circ - 80^\circ$ and $f^* = 0.12 - 0.16$. The highest efficiency of 32% is

achieved. Then the effects of the non-sinusoidal pitching motions are studied with both small pitching amplitudes and large pitching amplitudes considered.

We make a comparison between the effects of trapezoidal-like pitching profiles with small pitching amplitude ($\theta_0 = 45^\circ$) and large pitching amplitude ($\theta_0 = 75^\circ$). For small pitching amplitude, the trapezoidal-like pitching motion can indeed increase the energy harvesting efficiency. There exists an optimal value of β for each flapping frequency where the system can gain the highest energy harvesting efficiency. However, since $\theta_0 = 45^\circ$ is not the optimal pitching amplitude for the harvester, the highest efficiency obtained by varying β is still far below the highest efficiency obtained with sinusoidal pitching motion. As for the optimal pitching amplitude (large pitching amplitude cases), the performance improvement by tuning β is very limited. For $\theta_0 = 75^\circ$, the trapezoidal-like pitching profile can only improve the energy harvesting efficiency lightly for pitching frequency of $f^* = 0.12$. However for the most optimal pitching frequency ($f^* = 0.16$), the energy harvesting efficiency even drops as β increases. The increased efficiency with $f^* = 0.12$ is still a little lower than the highest frequency obtained with sinusoidal pitching profile, indicating a failure of increasing the upper boundary of energy harvesting efficiency by applying non-sinusoidal pitching motions. We conclude that the efficiency improvement strategy by using trapezoidal-like pitching profiles is ineffective in the range of optimal parameters.

The current study reminds us that it might be more appropriate to focus on the optimal operating parameters in a more extended parameter range, which would give us a comprehensive figure to design the performance improvement strategies, because most energy harvesters are expected to be working within a highest efficiency range. However, we note the trapezoidal-like pitching profile adopted in this paper and many previous studies can only represent one kind of many non-sinusoidal pitching strategies, with a natural defect of the derivative discontinuity in the pitching profile, and it cannot imitate vividly the flapping motion of animals' locomotive. Other non-sinusoidal pitching profiles such as adding in-line motion [25] are still worth further investigating. It is thus still an open question that if non-sinusoidal motions can actually increase the upper boundary of energy harvesting efficiency.

Acknowledgments

This research is supported by the National Natural Science Foundation of China (Grant No: 11272283) and Zhejiang Provincial Natural Science Foundation of China (Grant No: LY12A02006). D.P. gratefully acknowledges the support of Fundamental Research Funds for the Central Universities of China.

References

- [1] X.-M. Shao, D.-Y. Pan, Hydrodynamics of a flapping foil in the wake of a d-section cylinder, *J. Hydraul. Ser. B* 23 (4) (2011) 422–430.
- [2] T. Kinsey, G. Dumas, Testing and analysis of an oscillating hydrofoils turbine concept, in: ASME 2010 3rd Joint US-European Fluids Engineering Summer Meeting Collocated with 8th International Conference on Nanochannels, Microchannels, and Minichannels, American Society of Mechanical Engineers, 2010, pp. 9–22.
- [3] T. Wu, Extraction of Flow Energy by a Wing Oscillating in Waves, Tech. rep., National Technical Information Service, 1971.
- [4] T.Y. Wu, A.T. Chwang, Extraction of flow energy by fish and birds in a wavy stream, in: *Swimming and Flying in Nature*, Springer, 1975, pp. 687–702.
- [5] W. McKinney, J. Delauriert, The Wingmill : An Oscillating-Wing Windmill, *J. Energy* 5(2).
- [6] Q. Xiao, Q. Zhu, A review on flow energy harvesters based on flapping foils, *J. Fluids Struct.* 46 (2014) 174–191, <http://dx.doi.org/10.1016/j.fluidstructs.2014.01.002>.
- [7] J. Young, J.C. Lai, M.F. Platzer, A review of progress and challenges in flapping foil power generation, *Prog. Aerosp. Sci.* (2014) 1–27, <http://dx.doi.org/10.1016/j.paerosci.2013.11.001>.

- [8] K. Jones, M. Platzer, Numerical computation of flapping-wing propulsion and power extraction, *AIAA Pap.* 97 (1997) 0826.
- [9] G. Dumas, T. Kinsey, Eulerian simulations of oscillating airfoils in power extraction regime, *Adv. Fluid Mech.* VI (2006) 245.
- [10] B.J. Simpson, S. Licht, F.S. Hover, M.S. Triantafyllou, Energy extraction through flapping foils, in: *ASME 2008 27th International Conference on Offshore Mechanics and Arctic Engineering*, American Society of Mechanical Engineers, 2008, pp. 389–395.
- [11] T. Kinsey, G. Dumas, Parametric Study of an Oscillating Airfoil in a Power-Extraction Regime, *AIAA J.* 46 (6) (2008) 1318–1330, <http://dx.doi.org/10.2514/1.26253>.
- [12] T. Kinsey, G. Dumas, G. Lalande, J. Ruel, A. Méhut, P. Viarouge, J. Lemay, Y. Jean, Prototype testing of a hydrokinetic turbine based on oscillating hydrofoils, *Renew. Energy* 36 (6) (2011) 1710–1718, <http://dx.doi.org/10.1016/j.renene.2010.11.037>.
- [13] Q. Zhu, Optimal frequency for flow energy harvesting of a flapping foil, *J. Fluid Mech.* 675 (2011) 495–517, <http://dx.doi.org/10.1017/S0022112011000334>.
- [14] H. Cho, Q. Zhu, Performance of a flapping foil flow energy harvester in shear flows, *J. Fluids Struct.* (2014) 1–12, <http://dx.doi.org/10.1016/j.jfluidstructs.2014.08.007>.
- [15] X.-M. Shao, D.-Y. Pan, J. Deng, Z.-S. Yu, Numerical studies on the propulsion and wake structures of finite-span flapping wings with different aspect ratios, *J. Hydrom. Ser. B* 22 (2) (2010) 147–154.
- [16] J. Deng, C.P. Caulfield, X. Shao, Effect of aspect ratio on the energy extraction efficiency of three-dimensional flapping foils, *Phys. Fluids* 26 (4) (2014) 043102, <http://dx.doi.org/10.1063/1.4872224>.
- [17] Q. Zhu, Z. Peng, Mode coupling and flow energy harvesting by a flapping foil, *Phys. Fluids* 21 (3) (2009) 033601, <http://dx.doi.org/10.1063/1.3092484>.
- [18] Z. Peng, Q. Zhu, Energy harvesting through flow-induced oscillations of a foil, *Phys. Fluids* 21 (12) (2009) 123602, <http://dx.doi.org/10.1063/1.3275852>.
- [19] Q. Zhu, Energy harvesting by a purely passive flapping foil from shear flows, *J. Fluids Struct.* 34 (2012) 157–169, <http://dx.doi.org/10.1016/j.jfluidstructs.2012.05.013>.
- [20] J. Young, M.A. Ashraf, J.C.S. Lai, Numerical Simulation of Fully Passive Flapping Foil Power Generation, *AIAA J.* (2013) 1–13, <http://dx.doi.org/10.2514/1.J052542>.
- [21] G. Huxham, S. Cochard, J. Patterson, Experimental parametric investigation of an oscillating hydrofoil tidal stream energy converter, in: *Proceedings of 18th Australasian Fluid Mechanics Conference AFMC*, 2012.
- [22] J. Wu, Y.L. Qiu, C. Shu, N. Zhao, Pitching-motion-activated flapping foil near solid walls for power extraction: a numerical investigation, *Phys. Fluids* 26 (8) (2014) 083601, <http://dx.doi.org/10.1063/1.4892006>.
- [23] J. Wu, Y. Qiu, C. Shu, N. Zhao, An adaptive immersed boundary-lattice boltzmann method for simulating a flapping foil in ground effect, *Comput. Fluids* doi:10.1016/j.compfluid.2014.10.003.
- [24] S.C. Licht, M.S. Wibawa, F.S. Hover, M.S. Triantafyllou, In-line motion causes high thrust and efficiency in flapping foils that use power downstroke, *J. Exp. Biol.* (2010) 63–71, <http://dx.doi.org/10.1242/jeb.031708>.
- [25] J.S. Izraelevitz, M.S. Triantafyllou, Adding in-line motion and model-based optimization offers exceptional force control authority in flapping foils, *J. Fluid Mech.* 742 (2014) 5–34, <http://dx.doi.org/10.1017/jfm.2014.7>.
- [26] Q. Xiao, W. Liao, S. Yang, Y. Peng, How motion trajectory affects energy extraction performance of a biomimic energy generator with an oscillating foil? *Renew. Energy* 37 (1) (2012) 61–75, <http://dx.doi.org/10.1016/j.renene.2011.05.029>.
- [27] M. a. Ashraf, J. Young, J.C.S. Lai, M.F. Platzer, Numerical Analysis of an Oscillating-Wing Wind and Hydropower Generator, *AIAA J.* 49 (7) (2011) 1374–1386, <http://dx.doi.org/10.2514/1.J050577>.
- [28] K. Lu, Y. Xie, D. Zhang, Nonsinusoidal motion effects on energy extraction performance of a flapping foil, *Renew. Energy* 64 (2014) 283–293, <http://dx.doi.org/10.1016/j.renene.2013.11.053>.
- [29] Y. Xie, K. Lu, D. Zhang, Investigation on energy extraction performance of an oscillating foil with modified flapping motion, *Renew. Energy* 63 (2014) 550–557, <http://dx.doi.org/10.1016/j.renene.2013.10.029>.
- [30] M.F. Platzer, M. a. Ashraf, J. Young, S. Lecturer, Development of a New Oscillating-Wing Wind and Hydropower Generator, in: *New Horizons*, No. January, American Institute of Aeronautics and Astronautics, Orlando, Florida, 2009, pp. 1–13.
- [31] H. Jasak, *Error Analysis and Estimation for the Finite Volume Method with Applications to Fluid Flows* (Ph.D. thesis), Imperial College, University of London, 1996.
- [32] J.H. Ferziger, M. Perić, *Computational Methods for Fluid Dynamics*, Vol. 3, Springer, Berlin, 2002.
- [33] J. Deng, L. Teng, D. Pan, X. Shao, Inertial effects of the semi-passive flapping foil on its energy extraction efficiency, *Phys. Fluids* 27 (5) (2015) 053103, <http://dx.doi.org/10.1063/1.4921384>. <http://scitation.aip.org/content/aip/journal/pof2/27/5/10.1063/1.4921384>.